THE JOURNAL OF BIOLOGICAL CHEMISTRY VOL. 288, NO. 18, pp. 12805–12817, May 3, 2013
Published in the U.S.A.

Structural and Biochemical Characterization of *Plasmodium falciparum* 12 (*Pf*12) Reveals a Unique Interdomain Organization and the Potential for an Antiparallel Arrangement with *Pf*41*

Received for publication, January 22, 2013, and in revised form, March 18, 2013 Published, JBC Papers in Press, March 19, 2013, DOI 10.1074/jbc.M113.455667

Michelle L. Tonkin[‡1], Silvia A. Arredondo[§], Bianca C. Loveless[‡], Jason J. Serpa[¶2], Karl A. T. Makepeace[¶2], Natarajan Sundar[‖], Evgeniy V. Petrotchenko[¶2], Louis H. Miller[**], Michael E. Grigg[‖], and Martin J. Boulanger[‡3]

*From the [‡]Biochemistry and Microbiology, University of Victoria, Victoria, British Columbia, Canada V8W 3P6, [§]Laboratory of Immunogenetics and **Laboratory of Malaria and Vector Research, NIAID, National Institutes of Health, Rockville, Maryland 20852, [¶]University of Victoria Genome British Columbia Proteomics Centre, Biochemistry and Microbiology, University of Victoria, Victoria, British Columbia, Canada V8Z 7X8, and [‖]Molecular Parasitology Unit, Laboratory of Parasitic Diseases, NIAID, National Institutes of Health, Bethesda, Maryland 20892*

Background: *Pf*12 is the archetypal member of the 6-Cys protein family, members of which are important *Plasmodium* vaccine targets.
Results: Purifying selection and apical localization of *Pf*12, crystal structure of tandem 6-Cys domains, and mass spectrometry of cross-linked *Pf*12-*Pf*41 heterodimer are shown.
Conclusion: A functionally important role for *Pf*12 and potential for antiparallel heterodimer is provided.
Significance: First full-length 6-Cys protein structure and first details of heterodimer organization are revealed.

***Plasmodium falciparum* is the most devastating agent of human malaria. A major contributor to its virulence is a complex lifecycle with multiple parasite forms, each presenting a different repertoire of surface antigens. Importantly, members of the 6-Cys s48/45 family of proteins are found on the surface of *P. falciparum* in every stage, and several of these antigens have been investigated as vaccine targets. *Pf*12 is the archetypal member of the 6-Cys protein family, containing just two s48/45 domains, whereas other members have up to 14 of these domains. *Pf*12 is strongly recognized by immune sera from naturally infected patients. Here we show that *Pf*12 is highly conserved and under purifying selection. Immunofluorescence data reveals a punctate staining pattern with an apical organization in late schizonts. Together, these data are consistent with an important functional role for *Pf*12 in parasite-host cell attachment or invasion. To infer the structural and functional diversity between *Pf*12 and the other 11 6-Cys domain proteins, we solved the 1.90 Å resolution crystal structure of the *Pf*12 ectodomain. Structural analysis reveals a unique organization between the membrane proximal and membrane distal domains and clear homology with the SRS-domain containing proteins of *Toxoplasma gondii*. Cross-linking and mass spectrometry confirm the previously identified *Pf*12-*Pf*41 heterodimeric complex, and analysis of individual cross-links supports an unexpected antiparallel organization. Collectively, the localization and structure of *Pf*12 and details of its interaction with *Pf*41 reveal important insight into the structural and functional properties of this archetypal member of the 6-Cys protein family.**

Protozoan parasites in phylum Apicomplexa cause substantial morbidity and mortality worldwide. The most widely studied of these parasites are the *Plasmodium* species, the etiological agents of malaria. *Plasmodium falciparum* is of particular interest as the major cause of human malaria and is responsible for 0.8–1.2 million deaths every year (1, 2). Success of these parasites is based on a complex lifecycle supported by a sophisticated molecular arsenal of proteins that promotes infection, replication, and dissemination. Structural and functional characterization of stage-specific antigens in particular offers intriguing potential for vaccine and small molecule therapeutic development to limit the infectivity of these pathogens.

During the *Plasmodium* lifecycle, humans become infected with the sporozoite form of *P. falciparum* through the bite of an infected mosquito. Sporozoites migrate from the site of infection to the liver, where they invade hepatocytes, replicate, and differentiate into merozoites, which subsequently enter the blood stream and invade erythrocytes. After multiple rounds of asexual replication and rupture of the erythrocytes, most parasites re-invade in a cycle that leads to acute disease pathology, whereas some parasites differentiate into nonpathogenic sexual gametocytes. These gametocytes are taken up by a female *Anopheles* mosquito, where they undergo fertilization, invade

* This work was supported, in whole or in part, by Canadian Institutes of Health Research Grant MOP82915 (to M. J. B.). This work was also supported by the intramural funds of the NIAID, National Institutes of Health (to L. H. M.)
The atomic coordinates and structure factors (code 2YMO) have been deposited in the Protein Data Bank (http://wwpdb.org/).
[1] Supported by a Natural Sciences and Engineering Research Council of Canada Alexander Graham Bell Canada Graduate Scholarship (CGS-D3).
[2] Supported by a Genome Canada/Genome British Columbia Technology Development Grant.
[3] A Michael Smith Foundation for Health Research scholar and Canada Research Chair. To whom correspondence should be addressed: Biochemistry and Microbiology, University of Victoria, P. O. Box 3055 STN CSC, Victoria, BC, Canada V8W 3P6. Tel.: 250-721-7072; Fax: 250-721-8855; E-mail: mboulang@uvic.ca.

the midgut epithelium, and subsequently differentiate into sporozoites that travel to the salivary glands ready for transmission to a human host, thus completing the lifecycle.

During each lifecycle stage, various antigens coat the surface of the parasite. Among these, the 6-Cysteine (6-Cys) family of 12 s48/45 domain-containing proteins, originally identified in *Plasmodium* nearly 20 years ago (3), have garnered significant interest. Since their identification, 6-Cys domains have been found in proteins expressed on all *Plasmodium* lifecycle stages (4). More recently, homologues have been identified in all members of the aconoidasidan clade in the phylum Apicomplexa (5). The 6-Cys s48/45 domain is presented in copy numbers of 1–14 and generally in tandem pairs of A-type and B-type domains, termed *Plasmodium* gamete surface homology fragments (4). Of the 12 s48/45 domain-containing proteins in *P. falciparum* (5), only a select few have a known function. Two are essential to male/female gamete fusion (*Pf*s48/45 and *Pf*s230) (6–8), and one of these is also important for male gamete exflagellation and interaction with erythrocytes (*Pf*s230) (9), whereas others (*Pf*36 and *Pf*52) have roles in sporozoite infection of hepatocytes and replication therein (10, 11). Of note, *Pf*s230, which contains 14 s48/45 domains (7 *Plasmodium* gamete surface homology fragments), and *Pf*s48/45 are major transmission-blocking vaccine candidates (8, 12, 13), whereas *Pf*36 and *Pf*52 knockouts lead to attenuated parasites (11, 14–16). Four s48/45 family members are expressed on asexual blood stage parasites: *Pf*12, *Pf*38, *Pf*41, and *Pf*92. Importantly, *Pf*12, *Pf*38 and *Pf*41 are strongly recognized by immune sera from naturally infected patients (17–19). Although *Pf*12, *Pf*38, and *Pf*92 are associated with the membrane through a GPI[4] anchor (20), it was recently established that soluble *Pf*41 (17) heterodimerizes with *Pf*12 to maintain membrane association (21), similar to the association of soluble *Pf*s230 with GPI-anchored *Pf*s48/45 (7, 22). In addition, negative results were reported for *Pf*12 in erythrocyte binding assays, and the *Pf*12 knock-out showed normal invasion (21). Ultimately, no well defined functional role has yet been ascribed to any of the four blood-stage 6-Cys proteins.

*Pf*12 is the archetypal member of the s48/45 family of proteins, containing two s48/45 domains (4). The recently published NMR solution structure of the membrane proximal domain (domain 2 (D2); B-type) of *Pf*12 represents an important step toward describing the s48/45 domains (5). However, no structure of an A-type s48/45 domain or of a tandem pair has been reported, limiting our understanding of the natural presentation of these proteins on parasite surface membranes. Given that s48/45 domains are generally found in tandem repeats of A-type and B-type domains, elucidating the characteristics of the two domains together is important to fully understand this class of proteins. Additionally, based on studies of the homologous SAG1-related sequence (SRS) family from *Toxoplasma gondii* and related coccidians, the membrane distal domain (domain 1 (D1)) is likely to contain the functionally relevant region with respect to sensing host displayed molecules (23–27).

Defining the structural characteristics of a full-length 6-Cys protein from *Plasmodium* represents a key step toward characterizing this important family of proteins. To this end, we report the 1.90 Å resolution crystal structure of *Pf*12 that incorporates both D1 and D2 6-Cys domains. The structure reveals important insight into the domain organization and the potential for designing an effective blood stage vaccine. Insight into the functional importance of *Pf*12 is also shown through phylogenetic and cellular localization analysis, whereas cross-linking experiments coupled with mass spectrometry are used to investigate the architecture of the *Pf*12-*Pf*41 heterodimeric complex.

EXPERIMENTAL PROCEDURES

Polymorphism and Phylogenetic Analyses—6-Cys protein family member DNA sequences and strain-specific single nucleotide polymorphisms (SNPs) were downloaded from GenBank™ and PlasmoDB (13 isolates) (28) to calculate the ratio of synonymous to non-synonymous changes. To estimate ω (dN/dS ratio) the program PARRIS was used. $\omega > 1$ indicates positive (diversifying) selection, and $\omega < 0.5$ indicates purifying selection (29). All sequences were aligned using Clustal Omega (30) and subsequently edited manually in Jalview (31), and *Pv*38 (a 6-Cys ortholog) from *Plasmodium vivax* (AEZ68782.1) was selected as an appropriate outgroup for the *Pf*12 phylogenetic analysis. Phylogenetic tree reconstruction and evolutionary history among the 6-Cys DNA sequences were determined using neighbor-joining, maximum likelihood, and minimum evolution methods in MEGA5.0 (32) after deletion of gapped positions. Each phylogeny was tested using 1000 bootstrap replicates.

Preparation of P. falciparum Schizonts and Lysates—Synchronous cultures of *P. falciparum* 3D7 mature schizont-infected erythrocytes were purified on a Percoll/sorbitol gradient at 12,000 × *g* for 10 min at room temperature. For immunofluorescence assays, thin smears were prepared on glass slides, dried, and stored at −20 °C. For parasite lysates, 4×10^7 parasitized red blood cells (RBCs) were pelleted (2300 × *g* for 1 min) then resuspended in 1 ml of 0.15% saponin in 1× phosphate-buffered saline (PBS), centrifuged at 9000 × *g* for 1 min, and washed with 1 ml of 1× PBS before storage at −20 °C.

Antibody Generation and Testing—Antibodies against *Pf*12D2 (produced as previously described (5) and *Pf*12long (produced as described below) were generated in rabbits (Rockland Immunochemicals). After protein A purification of total IgG, the Pf12D2- and Pf12long-specific antibodies were affinity-purified using either a HiTrap NHS-activated HP column or NHS Mag-Sepharose (GE Healthcare) coupled to the respective protein according to the manufacturer's instructions. These antibodies were tested by Western blot analysis of parasite lysates. Briefly, the parasite pellet was incubated on ice in 100 μl of lysis buffer (50 mM Tris, pH 8.0, 150 mM NaCl, 5 mM EDTA, 0.5% Triton X-100, and Complete protease inhibitor (Roche Applied Science)) for 7 h. After removal of the insoluble fraction by centrifugation (16,000 × *g*), the soluble parasite lysate

[4] The abbreviations used are: GPI, glycophosphatidylinositol; 6-Cys, 6-cysteine; *Pf*12, *P. falciparum* P12; *Pf*41, *P. falciparum* P41; D1, domain 1; D2, domain 2; HBS, HEPES-buffered saline; CBDPS, CyanurBiotinDimercaptoPropionylSuccinimide; SRS, SAG1-related sequence; SNP, single nucleotide polymorphisms; TEV, tobacco etch virus; MBP, maltose binding protein.

was subjected to SDS-PAGE under reducing conditions and blotted onto a PVDF membrane. The membrane was probed with anti-Pf12D2 or anti-Pf12long (1.2 μg/ml) followed by goat anti-rabbit-HRP (0.08 μg/ml) (Jackson ImmunoResearch).

Antibody Labeling for Confocal Microscopy—The frozen schizont-infected RBC smears were equilibrated at room temperature and fixed by immersion in 1× PBS with 2.5% paraformaldehyde and 0.1% glutaraldehyde for 5 min. The samples were washed twice with 1× PBS and then blocked with 3% BSA, 0.1% Triton X-100 in PBS, pH 7.4, for 3 h. Incubation with primary antibodies diluted in blocking solution was done for 5 h followed by three 4-min washes with 0.1% Triton X-100 in PBS. The concentrations of the primary antibodies were affinity-purified rabbit anti-*Pf*12D2 or anti-*Pf*12long 12.4 μg/ml and mouse anti-RON4 mAb 24C6 2 μg/ml (33). The slides were then incubated with the corresponding labeled secondary antibodies (anti-rabbit Alexa 488 or anti-mouse Alexa 594) for 3 h and washed 3 times for 4 min. The samples were mounted with Vectashield Hard-Set with DAPI (Vector Labs) and allowed to polymerize at room temperature overnight. The images were generated by using a Zeiss LSM 710 confocal microscope, and brightness and contrast adjustments were made by Zen 2010 analysis software.

Expression and Purification of Pf12 2-domain Constructs for Antibody Production and Crystallization Using the Baculovirus System—A sequence encoding from the predicted signal peptide cleavage site to the GPI anchor site of *Pf*12 (His-26 to Ser-321, numbering is based on the initiation methionine in the signal sequence; *Pf*12long) was synthesized by GenScript, codon-optimized for insect cells, and subcloned into a modified pAcGP67b vector (Pharmingen) incorporating a C-terminal hexahistidine tag separated from *Pf*12 by a thrombin cleavage site. A second construct was subcloned that removed predicted regions of disorder at the N and C termini (Asn-28 to Ser-304; *Pf*12short).

The *Pf*12 encoding viruses for insect cell protein production were generated and amplified using established protocols (23, 24). For large-scale protein production, Hi5 insect cells were infected with amplified virus, and tunicamycin was added to a final concentration of 0.2 μg ml^{-1}. After a 48-h infection the supernatant was harvested, concentrated, buffer exchanged and allowed to batch-bind with nickel-Sepharose beads at 4 °C for 1 h. *Pf*12 was eluted with buffer containing 250 mM imidazole, and fractions were analyzed by SDS-PAGE and pooled based on purity. The hexahistidine tag was removed by thrombin cleavage, and the protein was further purified by size exclusion chromatography (HiLoad 16/60 Superdex 75; GE Healthcare) in HEPES-buffered saline (HBS) followed by an anion exchange pull-down to remove contaminating proteins.

Crystallization and Data Collection—Crystals of *Pf*12short grew after 1 month in 20 mM calcium chloride dihydrate, 20 mM cadmium chloride hydrate, 20 mM cobalt chloride hexahydrate, and 20% PEG 3350. The final drops consisted of 0.35 μl of protein (15 mg/ml) with 0.35 μl of reservoir solution and were equilibrated against 50 μl of reservoir solution. Cryo protection of the *Pf*12short crystal was carried out in mother liquor supplemented with 12.5% glycerol for 20 s and flash-cooled at 100 K directly in the cryo stream. Diffraction data were collected on beamline 9–2 at Stanford Synchrotron Radiation Lightsource.

TABLE 1
Data collection and refinement statistics for *Pf*12short
Values in parentheses are for the highest resolution shell.

Data collection	
Spacegroup	$P2_12_12_1$
a, *b*, *c* (Å)	41.66, 76.87, 85.05
α, β, γ (degree)	90, 90, 90
Wavelength (Å)	0.9795
Resolution range (Å)	42.52-1.90 (2.00-1.90)
Measured reflections	159,043
Unique reflections	22,181
Redundancy	7.2 (7.2)
Completeness (%)	99.8 (99.7)
$I/\sigma(I)$	16.1 (3.8)
R_{merge} [a]	0.058 (0.507)
Refinement statistics	
Resolution (Å)	42.50-1.90 (1.95-1.90)
R_{work} [b]/R_{free} [c]	0.240/0.289 (0.306/0.391)
No. of atoms	
Protein	1,772
Solvent	51
B values (Å^2)	
Protein	41.0
Solvent	44.4
Root mean square deviation from ideality	
Bond lengths (Å)	0.011
Bond angles (degree)	1.30
Ramachandran statistics (%)	
Most favored	94.8
Allowed	5.2
Disallowed	0.0

[a] $R_{merge} = \Sigma_{hkl}\Sigma_i|I_{hkl,i} - [I_{hkl}]|/\Sigma_{hkl}\Sigma_i I_{hkl,i}$, where $[I_{hkl}]$ is the average of symmetry-related observations of a unique reflection.
[b] $R_{work} = \Sigma|F_{obs} - F_{calc}|/\Sigma F_{obs}$, where F_{obs} and F_{calc} are the observed and the calculated structure factors, respectively.
[c] R_{free} is *R* using 5% of reflections randomly chosen and omitted from refinement.

Data Processing, Structure Solution, and Refinement—Diffraction data were processed using Imosflm (34) and Scala (35) in the CCP4 suite of programs (36). Initial phases for *Pf*12short were obtained by molecular replacement (MR) using PHASER (37) with the NMR solution structure of the membrane proximal domain (PDB ID 2LOE) (5) trimmed to remove mobile loops for D2 and a heavily trimmed poly-Ala model of the same domain generated using CHAINSAW (38) for D1. Solvent molecules were selected using COOT (39), and refinement was carried out using Refmac5 (40). Stereochemical analysis was performed with PROCHECK and SFCHECK in CCP4 (36). Overall, 5% of the reflections were set aside for calculation of R_{free}. Data collection and refinement statistics are presented in Table 1.

Accession Codes—The atomic coordinate and structure factor files for *Pf*12short have been deposited in the Protein Data Bank under the accession code 2YMO.

Expression and Purification of Pf12long(NXA) and Pf41(NXA) for Cross-linking and Mass Spectrometry—Sequences encoding *Pf*12long and *Pf*41 (Lys-21 to Ser-378) with all possible *N*-linked glycosylation sites knocked out by mutating Ser or Thr residues in the Asn-*X*-Ser/Thr (N*X*(S/T)) motif to alanine (N*X*A) were synthesized by GenScript, and the codons were optimized for insect cells and subcloned into a pAcSecG2T vector (Pharmingen) modified to contain an N-terminal hexahistidine tag and an MBP tag in place of the GST fusion, both separated from the protein of interest by a TEV protease cleavage site. The *Pf*12long(N*X*A)- and *Pf*41(N*X*A)-encoding viruses were gener-

ated and amplified and used for large scale protein production in Hi5 cells as described above, with the following exception; after overnight dialysis of nickel-purified MBP fusion protein into HBS_TEV (HBS with 0.5 mM EDTA, 3 mM reduced glutathione, 0.3 mM oxidized glutathione) and subsequent concentration, the MBP and His tags were cleaved by a 12–48-h incubation with TEV protease. The proteins were further purified by cation exchange chromatography to remove MBP followed by size exclusion chromatography in HBS with 2% glycerol.

Cross-linking and Mass Spectrometry Analysis of the Pf12long-(NXA) and Pf41(NXA) Heterodimer—Cross-linking analysis was performed using the isotopically coded collision-induced dissociation-cleavable affinity-purify-able cross-linker, CBDPS-H8/D8 (Creative Molecules, Inc.) and proteinase K digestion as described previously (41). *Pf*12long(N*X*A) and *Pf*41(N*X*A) in 1× PBS, pH 7.4, were cross-linked with 25 μM CBDPS-H8/D8 in PBS, and the samples were incubated for 30 min at 25 °C. The reaction mixtures were quenched with 25 mM ammonium bicarbonate for 30 min at 25 °C. Samples were reduced with 5 mM Tris(2-carboxyethyl)phosphine for 10 min at 25 °C and then treated with 10 mM iodoacetamide for 30 min at 37 °C in the dark followed by 10 mM DTT for 30 min at 37 °C. Cross-linked proteins were digested with proteinase K solution (Worthington, Lakewood, NJ) for 60 min at 37 °C at a 1:10 (w/w) enzyme:substrate ratio. Proteinase K was inhibited by the addition of 4-(2-aminoethyl)benzenesulfonyl fluoride and PMSF to a final concentration of 10 and 20 mM, respectively, and the cross-linked peptides were enriched on monomeric avidin beads (Thermo Scientific, Rockford, IL). The cross-links were eluted from the avidin beads with 0.1% TFA, 50% acetonitrile and concentrated by lyophilization. Mass spectrometric analysis was carried out with a nano-HPLC system (Easy-nLC II, ThermoFisher Scientific, Bremen, Germany) coupled to the electrospray ionization source of an LTQ Orbitrap Velos mass spectrometer (ThermoFisher Scientific). MS data were acquired with Mass Tags and Dynamic Exclusion enabled in global data-dependent settings (mass Δ: 4.02511, 2.68340, 2.01255; ratio range (%): 50–100). MS scans (m/z 400–2000 range) and MS/MS scans were acquired at 60,000 and 30,000 resolution, respectively. MSMS fragmentation was performed by collision-induced dissociation activation at a normalized collision energy of 35%. Data analysis was performed using DXMSMS Match of ICC-CLASS (42).

Homology Modeling of Pf41—To facilitate mapping of the cross-link positions, individual models of *Pf*41 D1 and *Pf*41 D2 were generated using a *Pf*12 D1 or D2 template, respectively. MUSCLE (43)-generated alignments were used as input for Modeler (44) within Chimera (45). A single model for each domain was chosen based on Modeler score and visual inspection.

RESULTS

Purifying Selection and Apical Localization of Pf12 Suggest an Important Functional Role—Although a definitive functional role for *Pf*12 is lacking (21), studies have shown that *Pf*12 is one of 11 proteins that make up >94% of the GPI-anchored proteome of schizont stage parasites (*Pf*12 ~ 5%) (20). To further investigate the functional consequences of *Pf*12, we performed bioinformatics and cellular localization studies.

Numerous *Plasmodium* surface proteins are highly polymorphic (46–50), including a majority of the 6-Cys proteins (4, 19, 51–53). To determine the evolutionary selection pressures acting on individual 6-Cys protein family members, we analyzed synonymous (dN) and non-synonymous (dS) polymorphisms among *P. falciparum* isolates to estimate the dN/dS ratio ω, which measures the strength of selection acting on a protein-coding gene, for *Pf*12, *Pf*38, *Pf*41, *Pf*s47, *Pf*s48/45, *Pf*52, *Pf*92, and *Pf*s230 (Fig. 1*A*). Only *Pf*12 was highly conserved and apparently under purifying selection ($\omega < 0.5$), supporting a conserved structural and central functional role for this protein, because it is under strong selective constraint from accumulating non-synonymous mutations despite its abundance and capacity to elicit antibody responses. In contrast, all other 6-Cys proteins displayed evidence of positive selection (genes that are under rapid diversification pressure either to escape host immunity or to evolve new function) whereby non-synonymous mutations are highly enriched ($\omega > 1$), as has been found previously for *Pf*s47, *Pf*s48/45, *Pf*s230, *Pf*38, and *Pf*92 (51, 54, 55). Sequence alignments and evolutionary phylogenetic analyses reveal that whereas many *P*12 proteins are also polymorphic (Fig. 1*B*), *Pf*12 is relatively non-polymorphic, and all non-synonymous changes in the ectoplasmic sequence are considered neutral (Fig. 1*B*, *inset*). These observations suggest an important function for *Pf*12 in *P. falciparum* biology and also highlight the evolutionary optimization of the *Pf*12 sequence that lacks deleterious mutations.

To investigate the cellular localization of *Pf*12 in mature schizonts, antibodies were generated against both *Pf*12long (Fig. 2*A*) produced in insect cells and the membrane proximal C-terminal domain (*Pf*12D2) produced in *Escherichia coli* (5). The antibodies were affinity-purified and tested for parasite protein recognition by Western blot analysis. Parasite lysates probed with either anti-*Pf*12D2 or anti-*Pf*12long show only a single band, migrating at the expected molecular weight in both cases (Fig. 2*B*). Immunofluorescent microscopy of purified mature schizonts labeled with anti-*Pf*12D2 indicates the presence of a clear punctate pattern (Fig. 2*C*). Although more diffuse, this pattern is also evident when labeling with anti-*Pf*12long. Simultaneous labeling of *Pf*RON4, a rhoptry neck protein (33), consistently shows adjacent localization to *Pf*12 with a significant degree of co-localization. These data indicate that in the late schizont stages, *Pf*12 is found in an apical organelle. This observation suggests a potential biological function in that apicomplexan proteins that share similar localization are involved in host cell invasion and the establishment of infection. It is noteworthy that a similar apical localization pattern has also been reported in mature schizonts for *Pv*12, the *P. vivax* orthologue (56), and in free merozoites for *Pf*12 (21).

Optimized Production of Full-length 6-Cys Proteins for Structural and Functional Analysis—A major challenge in studying the biochemistry of the 6-Cys family of proteins has been the difficulty in recombinantly producing properly folded, full-length proteins in large quantities. The majority of expression trials have relied on extensive refolding procedures (21, 57), the attachment of non-cleavable large fusion tags (3, 21, 58), com-

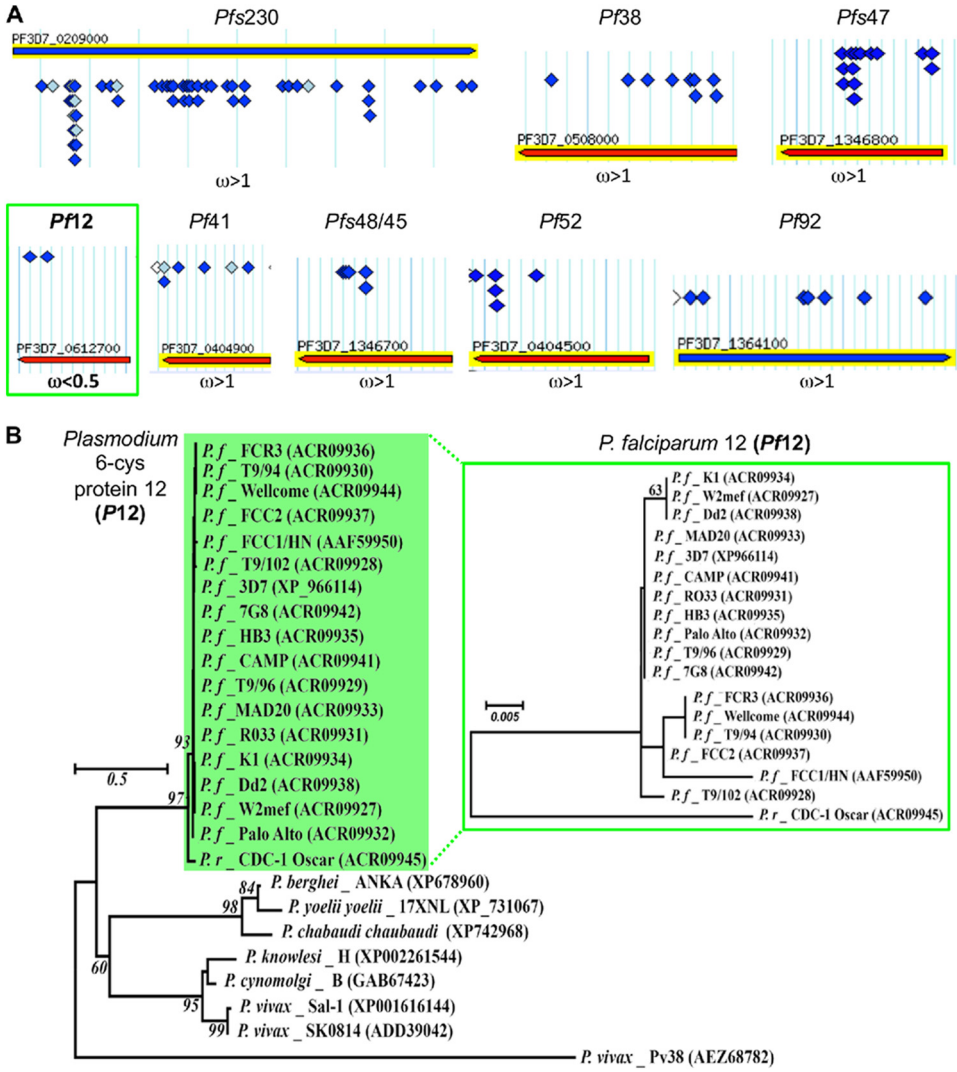

FIGURE 1. **Phylogenetic analysis of 6-Cys proteins from multiple *Plasmodium* species and strains reveals that *Pf*12 is under purifying selection.** *A*, allelic polymorphism and gene location for all SNPs are shown schematically for the following 6-Cys proteins: *Pf*s230, *Pf*38, *Pf*52, *Pf*41, *Pf*12, *Pf*s48/45, *Pf*s47, *Pf*92. Alleles were downloaded from among 13 *P. falciparum* isolates deposited in PlasmoDB Version 8.2). Alleles were derived from the following strains: 3D7 (The Netherlands); D6, RO-33, GHANA1, Senegal3404 (Africa); 7G8 (Brazil); D10, Dd2, FCC-2, K1, IT (Southeast Asia); HB3 (Honduras); SantaLucia (El Salvador). *Open diamond*, non-coding SNP; *light blue diamond*, synonymous SNP; *dark blue diamond*, non-synonymous SNP. ω (dN/dS ratio) was estimated using the PARRIS program; $\omega < 0.5$ indicated purifying selection, $\omega > 1$ indicated positive selection. *B*, the evolutionary history of *Pf*12 was inferred using maximum likelihood, minimum evolution neighbor joining methodology with 1000 bootstrap replications in the program MEGA5.0 from protein sequences downloaded from GenBank™ (accession numbers are shown in *parentheses*). A maximum likelihood tree is displayed. Isolate ID is included for each allele; *P.f* indicates *P. falciparum*, and *P.r* indicates *Plasmodium reichenowi*. The *inset* shows a higher resolution tree depicting *Pf*12 alleles present among 17 isolates collected globally.

plicated chaperone co-expression (59), detergent dependent extraction (12), or the production of fragments (5). Although each study substantially advanced the field, a more tractable expression system has the potential to facilitate structural analysis of the full-length molecules.

To this end we report two different successful strategies for producing full-length 6-Cys proteins. In the first strategy, a full-length construct of *Pf*12 extending from the signal peptide cleavage site to the GPI anchor site (*Pf*12long) and a second construct truncating short regions of predicted random coil at the N and C termini (*Pf*12short) (Fig. 2*A*) were produced as secreted His_6-fused proteins using the baculovirus insect cell system. To eliminate *N*-linked glycosylations and thereby mimic the predicted native state of the protein in *Plasmodium* (60), recombinant protein production was performed in the presence of tunicamycin. The secreted proteins were purified to homogeneity using Ni^{2+} affinity, size exclusion, and anion exchange chromatography. His tags were cleaved from both constructs, which eluted as monomers during gel filtration consistent with the recent characterization of a *Pf*12-ratCd4d3/4 fusion (21).

In the second strategy the production of *Pf*12 and its binding partner *Pf*41 were evaluated. Because both proteins contain numerous predicted *N*-linked glycosylation sites (*Pf*12, 8; *Pf*41, 7) and the expression in insect cells was severely attenuated in the presence of tunicamycin, we synthesized a full-length construct for each gene with the *N*-linked glycosylation sites mutated: *Pf*12long(N*X*A) and *Pf*41(N*X*A). Both proteins were expressed as secreted MBP fusions in the baculovirus insect cell system to facilitate the formation of soluble protein. After TEV-mediated cleavage of the MBP tag, cation exchange chromatography was followed by gel filtration chromatography as a final

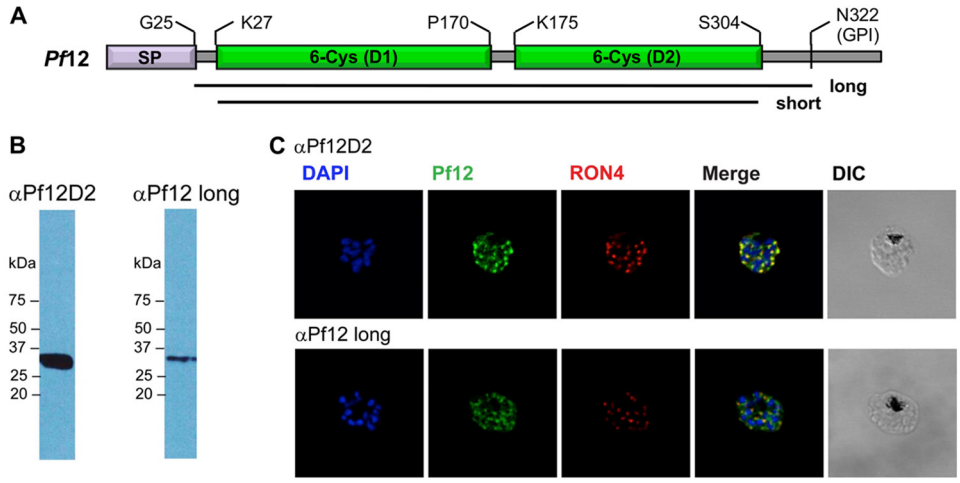

FIGURE 2. **Localization of *Pf*12 shows punctate apical staining with anti-*Pf*12D2 antibody and more diffuse staining with anti-*Pf*12long antibody.** *A*, shown is a schematic of *Pf*12 protein features and domain organization. *SP*, signal peptide; *D1*, membrane distal domain 1; *D2*, membrane proximal domain 2. *Horizontal black lines* indicate the two constructs used in this study, long (His-26 to Ser-321) and short (Asn-28 to Ser-304). *B*, shown is a Western blot analysis of late-schizont parasite lysates under reducing conditions. The amount of lysate in each lane is equivalent to 8×10^6 parasites. The membrane was probed with affinity-purified anti-*Pf*12D2 (1.2 μg/ml) or anti-*Pf*12long (1.2 μg/ml) followed by anti-rabbit-HRP antibodies. *C*, localization of *Pf*12 on mature schizonts is shown. Confocal microscopy images of purified late-schizont-infected RBCs are shown. The *top panel* shows labeling with affinity-purified anti-*Pf*12D2 (against C-terminal domain) and anti-RON4 antibodies. The *bottom panel* shows labeling with affinity-purified anti-*Pf*12long (against full-length) and anti-RON4 antibodies. *DIC*, differential interference contrast.

polishing step, and each protein eluted from the column as a single monomeric peak. Approximately 4 mg of highly purified, monodisperse protein for each of *Pf*12 and *Pf*41 was obtained per liter of culture.

Overall Structure—The ability to recombinantly produce properly folded, full-length 6-Cys proteins in milligram quantities enabled us to pursue structural characterization of the *Pf*12 and *Pf*41 ectodomains individually and in complex. Diffraction quality crystals were obtained for the *Pf*12short construct consisting of both D1 and D2 6-Cys domains with only the terminal coil shortened (Fig. 2*A*). The structure of *Pf*12short was solved to a resolution of 1.90 Å with one molecule in the asymmetric unit of the $P2_12_12_1$ unit cell. The final model begins at Leu-29 and extends through Ala-305 (from the expression tag; Ser-304 is the last native *Pf*12 residue modeled). By manual inspection and PISA software analysis (61), *Pf*12short crystallized as a monomer consistent with the elution profile from the gel filtration column. The tandem domains (D1 and D2) each adopt a β-sandwich fold and together measure ~75 Å in height and 43 Å at maximal width (Fig. 3*A*). The precise orientation of *Pf*12short with respect to the membrane is difficult to predict based solely on the structure, although studies of the related SRS superfamily from *T. gondii* suggest that the GPI-anchored D2 is located proximal to the membrane with D1 positioned away from the membrane poised for interaction with the host (23, 25). Analysis of the electrostatic and hydrophobic surfaces of *Pf*12short reveals a relatively even distribution of charged and non-polar residues across both domains.

Four regions of disorder are present in the *Pf*12short structure, all localized to surface loops projecting away from the core domain (*dotted lines* in Fig. 3*A* and 4*A*). In D1, a 33-residue region between Glu-83 and Ile-117 connecting β4 and β6 could not be modeled; this loop likely packs against both the side of D1 and across the bottom leaf of the β-sandwich, as observed in structures adopting the SRS fold (23–25). In addition, a 15-residue loop between Lys-142 (β7) and Asp-158 (β8) was disordered; the analogous loop in the SRSs is either shorter (*T. gondii* SAG1, 7 residues) or incompletely modeled (*Tg*BSR4, 10 residues; *Tg*SporoSAG, 19 residues). A sequence alignment with additional s48/45 family members reveals that this is a notably extended loop in *Pf*12 (4). Additionally, analysis of the crystal packing shows the β-sandwich of a neighboring molecule interfacing with the bottom leaf of the *Pf*12 D1 β-sandwich in the region predicted to be occupied by the two D1 loops in solution. In D2, two short regions could not be modeled unambiguously: a 5-residue region in the $\alpha1'$-$\beta3'$ (Lys-201 to Asn-205) loop, previously reported as a disordered loop by NMR (5), and a 3-residue segment between $\beta7'$ and $\beta8'$ (Glu-251 to Lys-253). Despite these regions of disorder, which led to high R_{free} values during refinement, the core fold of each domain was modeled with high confidence.

A Flexible Interdomain Linker Highlights the Potential for Mobility between D1 and D2—In the crystal lattice, the *Pf*12 D1 and D2 domains do not adopt a linear head-to-tail orientation but are rotated about the interdomain linker placing the central planes of the β sandwiches at ~45° to each other (Fig. 3*A*, *right*). The sequence of the D1-D2 linker does not contain structurally constrictive residues (SLNEK; Fig. 3*B*, *inset 1*), and there is no significant interface or hydrogen bonding interactions formed between D1 and D2, consistent with a complexation significance score of 0.0 (Fig. 3*B*, *inset 2*) (61). Taken together, these observations suggest that in solution and on the parasite membrane, there is the potential for mobility and reorganization of the *Pf*12 domains similar to the related BSR4 from *T. gondii* (23). This feature may affect the molecular surfaces available for interaction with its binding partner *Pf*41.

Topology and Connectivity of the Pf12 Tandem 6-Cys Domains—The D1 β-sandwich of *Pf*12 incorporates a 3-on-4 strand arrangement, with β1 forming part of the top leaf,

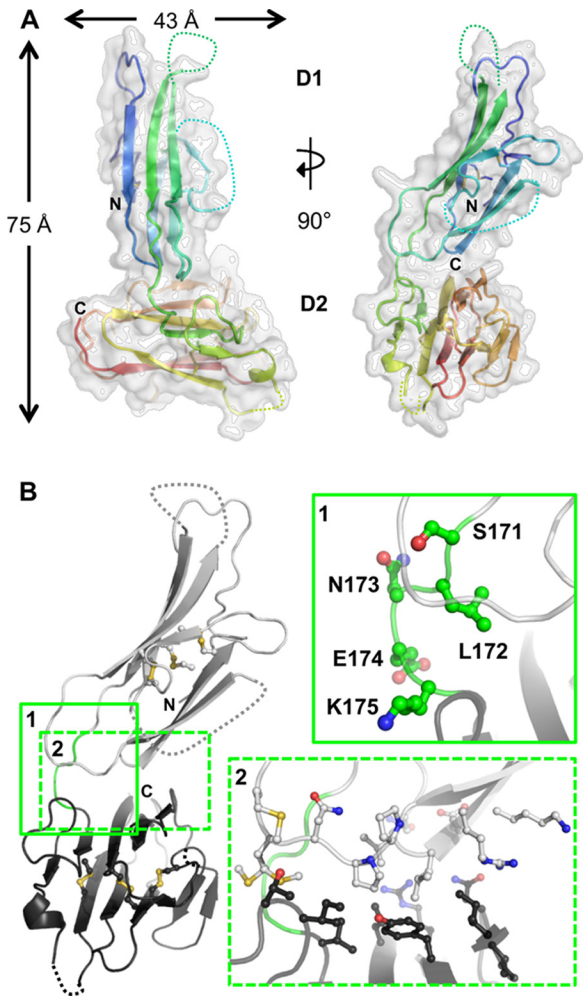

FIGURE 3. **Overall structure and interdomain organization of *Pf*12short.** *A*, shown are orthogonal views of the structure of *Pf*12short. The semi-transparent white surface reveals an overall size of ~75 Å tall by 43 Å wide. The secondary structure is shown beneath the surface as a schematic colored in a rainbow from the N terminus (*blue*) to the C terminus (*red*), with unmodeled regions indicated by *dotted connecting loops*. *B*, *inset 1*, analysis of the *Pf*12 inter-domain linker (Ser-171, Leu-172, Asn-13, Glu-174, and Lys-175) shows that no structurally constrictive or extremely hydrophobic residues are present. D1 is shown as *light gray*; *D2* is in *dark gray*; linker is in *green with side chains as balls* and *sticks*. *Inset 2*, interfacing residues (as defined by PISA software), shown as *balls* and *stick*, reveal the lack of a significant interface between D1 and D2. All molecular figures were generated in PyMOL.

whereas the membrane proximal D2 relies on a 5-on-4 strand arrangement for the core sandwich (Fig. 4*A*). Importantly, both sheets of the D1 and D2 β-sandwiches consist of parallel and antiparallel β-strands, distinguishing them from the purely antiparallel strands of the immunoglobulin fold. The modeled portion of D1 is composed solely of β-strands, whereas D2 is predominately β-strands with the addition of a single small α-helix positioned outside of the domain core (Fig. 4*A*). Three disulfide bonds are present in each domain with C1-C2, C3-C6, and C4-C5 connectivity (Fig. 4*A*, *right*). In both domains, C1-C2 and C3-C6 (Fig. 4*B*, *left*) pin together the two sheets of the β-sandwich, whereas C4-C5 links an ancillary loop to the core domain.

The 2-domain structure of *Pf*12 confirms the previous prediction for the disulfide bonding pattern of each domain (62) and is generally consistent with the original predicted β strand topology based off the structure of *Tg*SAG1 (4). The connection between D1 and D2 places the first β-strand (β1′) of the D2 domain next to β4′, and the β1′- β2′ turn loops around to place all three strands in parallel arrangement (Fig. 4, *A* and *B*, *right*), diverging from the mixed antiparallel and parallel prediction with β1′ on the outside edge (4) but consistent with the solution structure of *Pf*12 D2 (5). Importantly, this restricts the mobility of D2 and places the C terminus along the same end of D2 as the incoming tether from D1 (Fig. 4*A*, *right*). Overall, three possible orientations of *Pf*12 can be readily supported by our data (see Fig. 6*B*, *top*); 1) the organization observed in the crystal lattice, 2) the linker bent downward to maintain a nonlinear organization but with a more open conformation, or 3) the linker bent downward and subsequently rotated to provide an overall linear molecule but with the C terminus orientated toward D1.

Evolutionary Divergence between D1 and D2—To investigate the similarity of *Pf*12 to other structurally characterized proteins, a DaliLite search (63) was performed for *Pf*12 D1 and D2 separately. Consistent with the generally conserved β-sandwich core fold, the membrane distal D1 returned low but significant hits, with the primary result being the solution structure of *Pf*12 D2 (Z-score of 6.2). By comparison, a Z-score of 6.2 was also obtained with *Tg*BSR4 D1, likely due to the extended β-strands of this domain, similar to *Pf*12 D1. Other SRS domains gave scores between 5.1 and 5.7. *Pf*12 D2 gave significantly higher scoring hits, with the primary hit also being the solution structure of *Pf*12 D2, as expected (Z-score of 15.9). The remaining SRS domains gave scores between 9.9 and 10.5, whereas the highest similarity immunoglobulin domain scored 5.5.

Confirmation of the Pf12-Pf41 Heterodimeric Complex Formation—A recent study demonstrated that *Pf*12 and *Pf*41 form a heterodimeric complex on the surface of *P. falciparum* merozoites (21). Given the lysine-rich nature of both *Pf*12 (29 Lys, 9.6%; Fig. 5*A*) and *Pf*41 (40 Lys, 11%; Fig. 5*A*), we used primary amine cross-linking combined with mass spectrometry to confirm the *Pf*12-*Pf*41 interaction and to gain insights into the interaction interface.

Because the original experiments showing the interaction between recombinant *Pf*12 and *Pf*41 were performed with fusion proteins (Cd4d3/4 fusions (21)), we initially sought to confirm the interaction using our fusion-free proteins. *Pf*12long-(N*X*A) and *Pf*41(N*X*A) were incubated together in equimolar concentrations, and an increasing gradient of CBDPS cross-linker, a homobifunctional primary amine reactive cross-linker with a 14 Å spacer arm, was added to the solution. Subsequent gel electrophoresis of the samples showed a clear band of increasing intensity at the expected size of the cross-linked product (*Pf*12long(N*X*A)[34.1 kDa] + *Pf*41(N*X*A)[41.2 kDa] = 75.3 kDa) (data not shown). MALDI-TOF analysis of a tryptic digest of the cross-linked product clearly showed the presence of peptides from both proteins (Fig. 5*A*).

Pf12-Pf41 Cross-link Identification—Having confirmed that our recombinant *Pf*12 and *Pf*41 form a heterodimeric complex, the cross-linking conditions were optimized (Fig. 5*B*), and the cross-linked sample was digested with proteinase K and analyzed by tandem mass spectrometry (MS/MS) to identify cross-linked peptides.

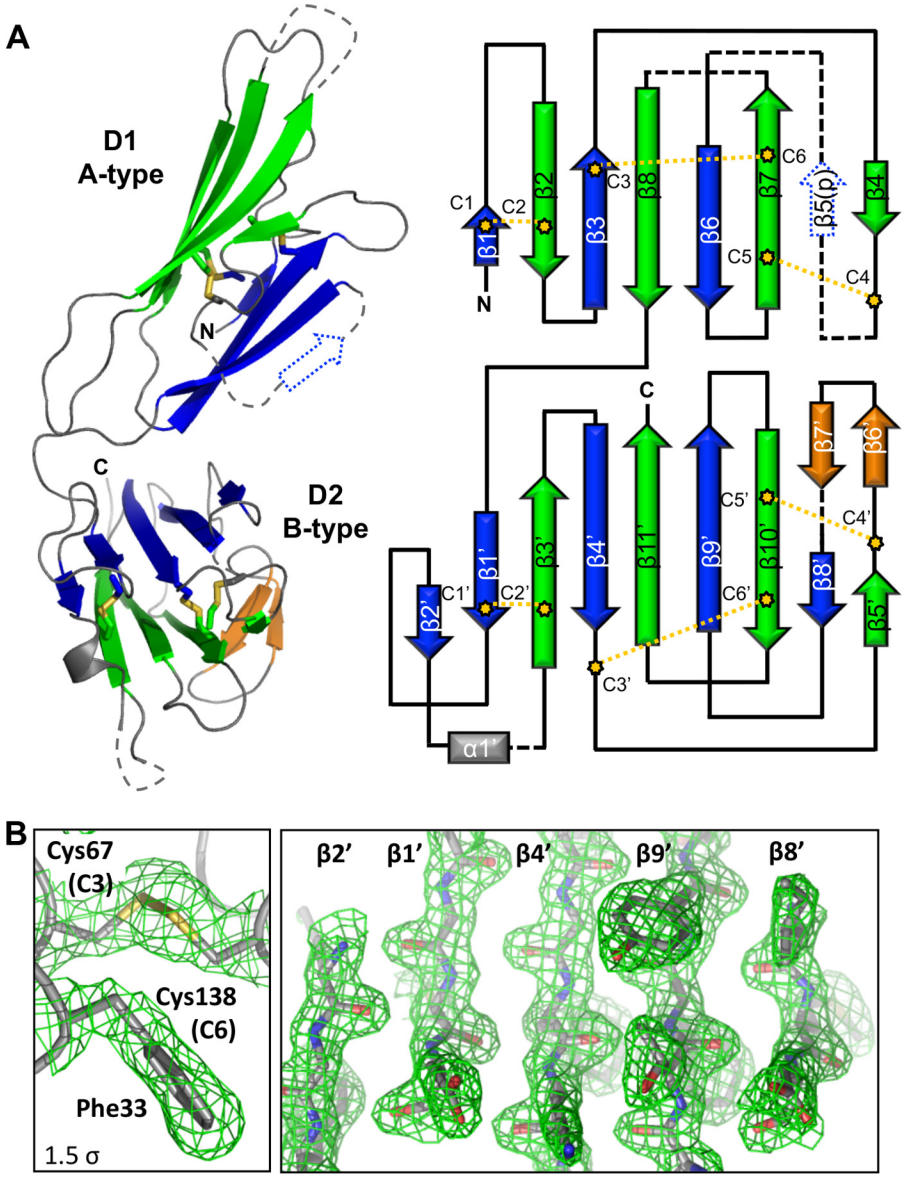

FIGURE 4. **Topology and disulfide connectivity of *Pf*12short.** *A*, *left*, shown is a schematic representation of *Pf*12short with the β-strands of the top leaf of each β-sandwich, colored *blue*, and of the bottom leaf, colored *green*. Two β-stands in an ancillary loop of D2 are colored *orange*. Disulfides are shown as *yellow sticks*. *Dotted lines* indicate unmodeled regions and predicted features. *Right*, shown is a topology diagram of *Pf*12short, colored as in the *left*. *β5(p)* indicates a predicted β-strand based on other similar structures. *B*, shown are electron density maps (*green mesh*), contoured at 1.5 σ, of the Cys-67—Cys-138 (C3-C6) linkage in *Pf*12short D1 (*left*) and of the top leaf of the *Pf*12short D2 β-sandwich (*right*).

*Pf*12-*Pf*12 (intra-protein links), *Pf*41-*Pf*41 (intra-protein links), and *Pf*12-*Pf*41 (inter-protein) cross-links were all identified with high confidence (Table 2). Of the eight unique cross-links found within *Pf*12 (Table 2), all of them agree with the structural data presented: seven D1-D1 cross-links predominantly in flexible loops were observed along with 1 D2-D2 cross-link, but no inter-domain cross-links were found, consistent with our observation of an insignificant interface between the tandem domains of *Pf*12 (Fig. 3*B*).

Thirty-seven unique intra-molecular cross-links were observed for *Pf*41 (Table 2), spanning the different regions of the protein, which include two s48/45 domains separated by a long linker region that lacks strongly predicted secondary structure elements: 6 within D1, 13 between D1 and the linker, 3 between D1 and D2, 7 within the linker, 4 between the linker and D2, and 4 within D2. Together, these cross-links suggest that *Pf*41 is compact in solution, and a selection of mutually exclusive cross-links is consistent with a degree of flexibility in solution enabled by its modular nature and long linker. In particular, based on our homology models of the *Pf*41 6-Cys domains, the 29–333 and 59–323 cross-links (Table 2) suggest that D2 is above the apical surface of D1, whereas the 146–252/264/275/327 cross-links (Table 2) suggest that the D1 to linker transition region at the base of D1 is located next to D2 (Fig. 6*B*, *middle*).

Of the 21 unique *Pf*12-*Pf*41 cross-links observed (Table 2), 7 are between *Pf*12 D1 and either *Pf*41 D2 or a C-terminal peptide, 4 are between *Pf*12 D1 and *Pf*41 linker, 2 are between *Pf*12 D1 and *Pf*41 D1, 5 are between *Pf*12 D2 and *Pf*41 D1, 2 are between *Pf*12 D2 and *Pf*41 linker, and 1 is

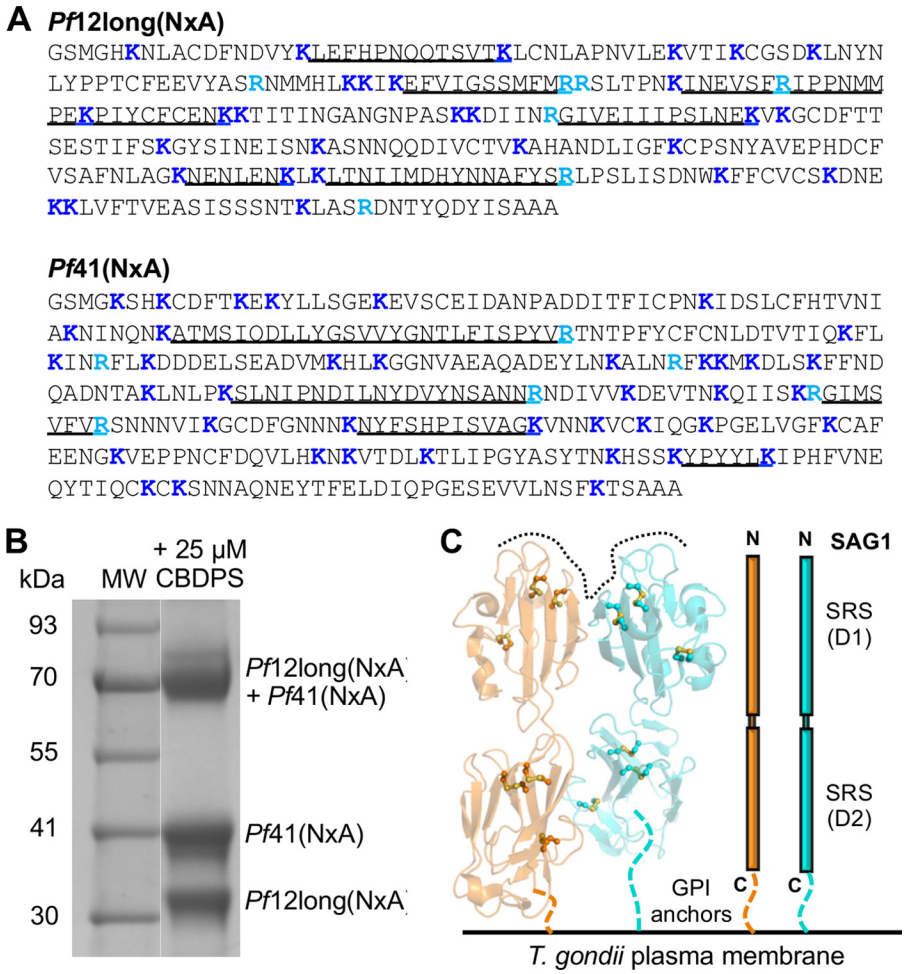

FIGURE 5. **Cross-linking optimization and expected parallel dimer outcome.** *A*, shown are sequences of *Pf*12long(N*X*A) and *Pf*41(N*X*A), with the highest abundance identified peptides *underlined*. Lysine residues are highlighted in *dark blue*, and arginine residues are in *light blue*. *B*, SDS-PAGE analysis of the optimized cross-linking reaction used for the proteinase K solution digest shows the expected migration pattern for *Pf*12long(N*X*A), *Pf*41(N*X*A), and the cross-linked heterodimer. *C*, SAG1 homodimer from *T. gondii* (1KZQ). *Left*, shown is a schematic representation of the homodimer shown in the predicted orientation to the parasite membrane, with one monomer colored *orange* and the second monomer colored *cyan*. Three disulfide bonds in each domain are shown as *yellow balls* and *sticks*. GPI anchors are indicated by colored *dashed lines*, and the predicted ligand binding surface generated at the homodimeric interface is indicated by a *black dotted line*. *Right*, shown is a schematic of the parallel organization of the *Tg*SAG1 homodimer enforced by the presence of GPI anchors.

between *Pf*12 D2 and *Pf*41 D2. Clearly, the lack of predominant D1-D1 and D2-D2 cross-links does not support the parallel dimer organization observed with the *T. gondii* SRS homodimers (Fig. 5*C*) (23, 25).

DISCUSSION

Predicted Organization of Pf12 D1 and D2 on the Parasite Membrane—Due to the possible mobility in the D1-D2 linker region (Fig. 3*B*), the positioning of the C terminus in the crystal structure, which is well ordered and directed toward D1 (Fig. 4*A*, *left*), and the extended linker region between D2 and the GPI anchor site (17 residues not included in the crystallization construct), it is difficult to predict the disposition of *Pf*12 on the membrane of the parasite other than the proximity of D2 due to its GPI anchor. In addition, tight crystal packing likely contributes to the relative orientation of the two domains observed in the crystal structure. However, despite the predicted inherent flexibility of the linker, the parallel arrangement of the first two β-strands in D2, with the first strand pinned by a disulfide bond (Fig. 4*A*), suggest that although D1 may be free to rotate, the lack of a head-to-tail organization of the two domains is a true feature of *Pf*12. More specifically, the top leaf of D2 restricts the ability of *Pf*12 to align with D1 orientated distal to the C terminus as has been observed for the SRS proteins (23–25).

The SRS-like Fold of s48/45 Domains—The SRS fold was originally defined based on the structure of *Tg*SAG1 (25) and has since been refined with structural characterization of *Tg*BSR4 (23) and *Tg*SporoSAG (24) as well as bioinformatics analyses (27, 64–67). The *Plasmodium* s48/45 domains were previously predicted to adopt a fold similar to the coccidian SRS proteins despite showing only 5–9% primary sequence identity (4). The recent solution structure of *Pf*12 D2 confirmed that this domain contains an SRS-like fold (5). SRS and s48/45 domains are both β-sandwich domains with a mixture of parallel and antiparallel strands, separating them from the immunoglobulin fold of purely antiparallel strands. However, a major reason that the s48/45 domains are not considered to adopt a true SRS fold is the differences in disulfide bond connectivity. All SRSs characterized to date have C1-C6, C2-C5, C3-C4

TABLE 2

Unique primary NXA amine cross-links from an in-solution proteinase K digest of CBDPS-cross-linked *Pf*12long (N*X*A) and *Pf*41 (N*X*A)

Cross-links designated in light grey and italics in the *Pf*12-*Pf*41 column, do not have a straightforward agreement with an anti-parallel model.

N, N-terminal peptide; D2-GPI, short region between domain 2 and GPI anchor site; L, linker; C, C-terminal peptide.

*Pf*12-*Pf*12		*Pf*41-*Pf*41		*Pf*12-*Pf*41	
22 **(N)**	27 **(D1)**	29 **(D1)**	31 **(D1)**	27 **(D1)**	376 **(C)**
51 **(D1)**	66 **(D1)**	-	146 **(L)**	51 **(D1)**	304 **(D2)**
95 **(D1)**	132 **(D1)**	-	333 **(D2)**	66 **(D1)**	275 **(D2)**
-	141 **(D1)**	31 **(D1)**	143 **(D1)**	-	376 **(C)**
141 **(D1)**	156 **(D1)**	-	146 **(L)**	71 **(D1)**	167 **(L)**
-	157 **(D1)**	38 **(D1)**	72 **(D1)**	-	174 **(L)**
142 **(D1)**	156 **(D1)**	-	78 **(D1)**	-	190 **(L)**
214 **(D2)**	308 **(D2-GPI)**	-	146 **(L)**	-	216 **(L)**
		59 **(D1)**	190 **(L)**	96 **(D1)**	*29 **(D1)***
		-	323 **(D2)**	-	304 **(D2)**
		78 **(D1)**	146 **(L)**	132 **(D1)**	304 **(D2)**
		-	252 **(D2)**	156 **(D1)**	376 **(C)**
		122 **(D1)**	131 **(D1)**	157 **(D1)**	125 **(D1)**
		-	170 **(L)**	214 **(D2)**	143 **(D1)**
		-	174 **(L)**	246 **(D2)**	29 **(D1)**
		-	185 **(L)**	-	31 **(D1)**
		-	190 **(L)**	-	143 **(D1)**
		125 **(D1)**	131 **(D1)**	-	167 **(L)**
		-	190 **(L)**	253 **(D2)**	143 **(D1)**
		131 **(D1)**	146 **(L)**	-	*252 **(D2)***
		-	190 **(L)**	288 **(D2)**	146 **(L)**
		143 **(D1)**	146 **(L)**		
		146 **(L)**	174 **(L)**		
		-	185 **(L)**		
		-	216 **(L)**		
		-	252 **(D2)**		
		-	264 **(D2)**		
		-	275 **(D2)**		
		-	327 **(D2)**		
		161 **(L)**	174 **(L)**		
		-	190 **(L)**		
		174 **(L)**	185 **(L)**		
		-	190 **(L)**		
		252 **(D2)**	264 **(D2)**		
		-	327 **(D2)**		
		264 **(D2)**	275 **(D2)**		
		304 **(D2)**	306 **(D2)**		

disulfide connectivity (23–25), whereas both A-type and B-type domains of s48/45 proteins, as shown with the structure of *Pf*12, adopt a C1-C2, C3-C6, C4-C5 type connectivity (Fig. 3*A*). As previously noted for *Pf*12, two disulfides pin together the two leafs of the β-sandwich, whereas the third disulfide pins an ancillary loop to the core domain. This is in contrast to the SRSs, where two disulfides also pin together the β-sandwich, but the third disulfide, with the exception of *Tg*SporoSAG D2, pins an ancillary loop to itself (23–25). Furthermore, members of the SRS superfamily generally have a selection of conserved residues and at least 20% sequence identity (27, 64–66, 68), but members of the s48/45 family do not meet these criteria, with generally <10% sequence identity. The DaliLite search performed further supports the conclusion that *Pf*12 adopts an SRS-like fold, as each *Pf*12 domain gave a significant Z-score with the SRS domains (5.1–10.5) but lower scores than are obtained when searching the database with *Tg*SAG1, the prototypical member of the SRS superfamily, which has Z-scores of 11.9–17.1 with other SRS-fold-containing proteins. These results underpin the structural diversity encompassed by the SRS fold, which exists as a multifunctional scaffold for the taxa-specific evolution of surface coat proteins within the Apicomplexa (23–25).

Implications for the Pf12-Pf41 Heterodimeric Complex—Although a selection of SRS proteins apparently exists as parallel homodimers on the parasite surface through GPI anchor-mediated clustering to generate functional ligand binding surfaces (Fig. 5*C*) (23, 25, 26), previous modeling of *Pf*12 as a potential homodimer did not reveal any functional insights (4). However, a recent study revealed that GPI-anchored *Pf*12 forms a heterodimeric complex with soluble *Pf*41 (21). In particular, this work showed co-elution of the two proteins on a size exclusion column and measured an SPR-based K_d for the interaction of 310 nM. The structural elucidation of the *Pf*12-*Pf*41 complex will provide valuable insight into the molecular recognition between two different 6-Cys proteins and may ultimately support their functional characterization (21).

We have presented here the structure of the D1 and D2 tandem domains of *Pf*12 (Figs. 3 and 4), which is the first full-length structure of a 6-Cys protein. Although homology modeling of the individual *Pf*41 6-Cys domains using separated D1 and D2 templates was successful (Fig. 6*A*, *right*), it is important to note that the boundary between *Pf*41 D1 and the linker region is ambiguous, which impacts the predicted length of the β7-β8 loop and, therefore, also the composition of β8 and the length of the linker. Also, the *Pf*41 linker region does not contain any identifiable motifs, and no suitable template for modeling could be identified. Finally, the possible mobility between the three *Pf*41 regions renders the use of traditional modeling techniques unsuitable. We, therefore, undertook a cross-linking combined with a mass spectrometry approach to investigate the interdomain organization of *Pf*41 and determine key features of the interaction interface of the *Pf*12-*Pf*41 heterodimeric complex.

In contrast to *Pf*12, for which no inter-domain cross-links were found (Table 2), several cross-links between *Pf*41 D1 and *Pf*41 D2 were identified as well as links between *Pf*41 D1 and the extended linker region. The high number of cross-links between different regions of *Pf*41 D1 and various parts of the linker (Table 2) suggest that these regions are closely associated in solution and that the linker is not fully extended (Fig. 6*B*, *middle*). Importantly, the contrast between the number of intra-molecular cross-links for *Pf*12 (8) and *Pf*41 (37) does not correlate with the number of lysine residues available for cross-linking (*Pf*12long(N*X*A), 29; *Pf*41(N*X*A), 40; Fig. 5*A*) but rather suggests more intimate interdomain interfaces for *Pf*41.

Although other observed dimers between SRS domain-harboring proteins, SAG1 and BSR4 homodimers, adopt a parallel organization, the lack of a GPI anchor on *Pf*41 (17) provides the intriguing possibility that the *Pf*12-*Pf*41 heterodimer is not constrained to such an arrangement. Indeed, the cross-links identified between *Pf*12 and *Pf*41 support an antiparallel arrangement of the two proteins (Fig. 6, *A* and *B*, *bottom*), with clear cross-links between *Pf*12 D1 and *Pf*41 D2, and between *Pf*12 D2 and *Pf*41 D1. Only two cross-links do not have a straightforward connection to an antiparallel organization, leaving the possibility that additional less abundant conformations exist in solution. Of additional interest, the only cross-links between *Pf*12

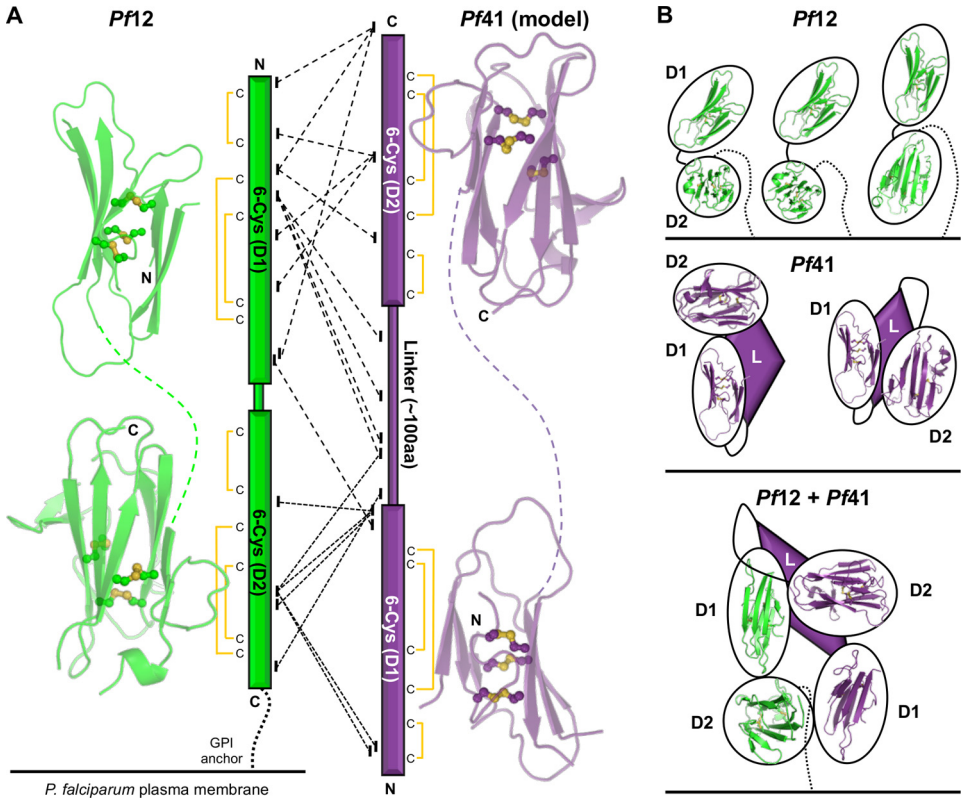

FIGURE 6. **Mass spectrometry and cross-linking confirm the *Pf*12-*Pf*41 heterodimeric interaction and suggest an antiparallel organization.** *A*, *left*, shown is the *Pf*12 structure split into D1 and D2, highlighting the β-sandwich core (*green schematic*) and three disulfides (*yellow balls* and *sticks*) in each domain. Linker is shown as a *green dashed line*. *Center*, shown is a graphical representation of MS/MS results from analysis of the cross-linked *Pf*12long(N*X*A)-*Pf*41(N*X*A) heterodimer. Cross-links supporting the potential for an antiparallel organization, enabled by the lack of a *Pf*41 GPI anchor, are shown as *dashed* (emanating from *Pf*12 D1) and *dotted* (emanating from *Pf*12 D2) *lines*. Disulfide connectivity is indicated. *Right*, *Pf*41 D1 and D2 models generated off *Pf*12short D1 and D2 templates, respectively, highlighting the β-sandwich core (*purple schematic*) and three disulfides (*yellow balls* and *sticks*) in each domain. The linker is shown as a *purple dashed line*. *B*, schematics of the most likely organizations of *Pf*12 (*top*, *green*), *Pf*41 (*middle*, *purple*), and the *Pf*12-*Pf*41 complex are based on structural and cross-linking data. GPI anchors are shown as *dotted lines*. *Pf*41 linker with unknown structural elements are shown as *purple diamonds*. *Black ovals* around structurally characterized domains (*Pf*12 D1 and D2) and homology modeled domains (*Pf*41 D1 and D2) are presented for clarity of the general organization due to the uncertainty in the exact interacting molecular surfaces.

D1 and the *Pf*41 linker region originate from a single lysine in the β3-β4 *Pf*12 apical loop, suggesting that the *Pf*41 linker may form an integral part of the molecular surface presented to the host environment (Fig. 6*B*, *bottom*). This is supported by a previous study showing that human immune sera reacted with a recombinantly expressed portion of *Pf*41 encompassing the majority of the linker region (17) and may help to explain why *Pf*12 is under purifying selection, in contrast to the other 6-Cys protein family members that are under positive selection, likely driven by adaptive immunity and/or mating interactions (among the 6-Cys gamete surface proteins).

Conclusion—Overall, our phylogenetic and localization data suggest that *Pf*12, the archetypal 6-Cys family member, is optimized for a functional role in *P. falciparum*. The structure of *Pf*12short is the first of a full-length 6-Cys protein with both the A-type and B-type domains making up the *Plasmodium* gamete surface homology fragment observed as the core of the 6-Cys protein family members, including the major transmission blocking vaccine candidates *Pf*s230 and *Pf*s48/45, and shows that *Pf*12 has an SRS-like fold and a unique orientation between the two s48/45 domains. Furthermore, our cross-linking and mass spectrometry data not only confirm the interaction between *Pf*12 and *Pf*41 but also suggest an unexpected antiparallel organization between the two proteins facilitated by the lack of a GPI anchor on *Pf*41, which holds clear implications for the molecular surface presented to the host cell.

Acknowledgments—We gratefully acknowledge the staff at the Stanford Synchrotron Radiation Lightsource. We thank Prakash Srinivasan and Julia Knoeckel (Laboratory of Malaria Vector Research, National Institutes of Health (NIH)) for training and helpful discussions, Joseph Brzostowski (Laboratory of Immunogenetics, NIH) for assistance with confocal imaging, and Jean-François Dubremetz for antibody 24C6 (RON4). We thank the beamline staff at Stanford Synchrotron Radiation Lightsource.

REFERENCES

1. World Health Organization. (2010) World Malaria Report, World Health Organization, Geneva, Switzerland
2. Murray, C. J., Rosenfeld, L. C., Lim, S. S., Andrews, K. G., Foreman, K. J., Haring, D., Fullman, N., Naghavi, M., Lozano, R., and Lopez, A. D. (2012) Global malaria mortality between 1980 and 2010. A systematic analysis. *Lancet* **379,** 413–431
3. Williamson, K. C., Criscio, M. D., and Kaslow, D. C. (1993) Cloning and expression of the gene for *Plasmodium falciparum* transmission-blocking target antigen, Pfs230. *Mol. Biochem. Parasitol.* **58,** 355–358
4. Gerloff, D. L., Creasey, A., Maslau, S., and Carter, R. (2005) Structural models for the protein family characterized by gamete surface protein Pfs230 of *Plasmodium falciparum*. *Proc. Natl. Acad. Sci. U.S.A.* **102,**

13598–13603
5. Arredondo, S. A., Cai, M., Takayama, Y., MacDonald, N. J., Anderson, D. E., Aravind, L., Clore, G. M., and Miller, L. H. (2012) Structure of the *Plasmodium* 6-Cysteine s48/45 domain. *Proc. Natl. Acad. Sci. U.S.A.* **109,** 6692–6697
6. van Dijk, M. R., Janse, C. J., Thompson, J., Waters, A. P., Braks, J. A., Dodemont, H. J., Stunnenberg, H. G., van Gemert, G. J., Sauerwein, R. W., and Eling, W. (2001) A central role for P48/45 in malaria parasite male gamete fertility. *Cell* **104,** 153–164
7. Kumar, N. (1987) Target antigens of malaria transmission-blocking immunity exist as a stable membrane-bound complex. *Parasite Immunol.* **9,** 321–335
8. Williamson, K. C. (2003) Pfs230. From malaria transmission-blocking vaccine candidate toward function. *Parasite Immunol.* **25,** 351–359
9. Eksi, S., Czesny, B., van Gemert, G. J., Sauerwein, R. W., Eling, W., and Williamson, K. C. (2006) Malaria transmission-blocking antigen, Pfs230, mediates human red blood cell binding to exflagellating male parasites and oocyst production. *Mol. Microbiol.* **61,** 991–998
10. van Schaijk, B. C., Janse, C. J., van Gemert, G. J., van Dijk, M. R., Gego, A., Franetich, J. F., van de Vegte-Bolmer, M., Yalaoui, S., Silvie, O., Hoffman, S. L., Waters, A. P., Mazier, D., Sauerwein, R. W., and Khan, S. M. (2008) Gene disruption of *Plasmodium falciparum* p52 results in attenuation of malaria liver stage development in cultured primary human hepatocytes. *PLoS One* **3,** e3549
11. VanBuskirk, K. M., O'Neill, M. T., De La Vega, P., Maier, A. G., Krzych, U., Williams, J., Dowler, M. G., Sacci, J. B., Jr., Kangwanrangsan, N., Tsuboi, T., Kneteman, N. M., Heppner, D. G., Jr., Murdock, B. A., Mikolajczak, S. A., Aly, A. S., Cowman, A. F., and Kappe, S. H. (2009) Preerythrocytic, live-attenuated *Plasmodium falciparum* vaccine candidates by design. *Proc. Natl. Acad. Sci. U.S.A.* **106,** 13004–13009
12. Chowdhury, D. R., Angov, E., Kariuki, T., and Kumar, N. (2009) A potent malaria transmission blocking vaccine based on codon harmonized full-length Pfs48/45 expressed in *Escherichia coli*. *PLoS One* **4,** e6352
13. Quakyi, I. A., Carter, R., Rener, J., Kumar, N., Good, M. F., and Miller, L. H. (1987) The 230-kDa gamete surface protein of *Plasmodium falciparum* is also a target for transmission-blocking antibodies. *J. Immunol.* **139,** 4213–4217
14. van Dijk, M. R., Douradinha, B., Franke-Fayard, B., Heussler, V., van Dooren, M. W., van Schaijk, B., van Gemert, G. J., Sauerwein, R. W., Mota, M. M., Waters, A. P., and Janse, C. J. (2005) Genetically attenuated, P36p-deficient malarial sporozoites induce protective immunity and apoptosis of infected liver cells. *Proc. Natl. Acad. Sci. U.S.A.* **102,** 12194–12199
15. Waters, A. (2006) Malaria. New vaccines for old? *Cell* **124,** 689–693
16. van Schaijk, B. C., Vos, M. W., Janse, C. J., Sauerwein, R. W., and Khan, S. M. (2010) Removal of heterologous sequences from *Plasmodium falciparum* mutants using FLPe-recombinase. *PLoS One* **5,** e15121
17. Sanders, P. R., Gilson, P. R., Cantin, G. T., Greenbaum, D. C., Nebl, T., Carucci, D. J., McConville, M. J., Schofield, L., Hodder, A. N., Yates, J. R., 3rd, and Crabb, B. S. (2005) Distinct protein classes including novel merozoite surface antigens in Raft-like membranes of *Plasmodium falciparum*. *J. Biol. Chem.* **280,** 40169–40176
18. Elliott, J. F., Albrecht, G. R., Gilladoga, A., Handunnetti, S. M., Neequaye, J., Lallinger, G., Minjas, J. N., and Howard, R. J. (1990) Genes for *Plasmodium falciparum* surface antigens cloned by expression in COS cells. *Proc. Natl. Acad. Sci. U.S.A.* **87,** 6363–6367
19. Reeder, J. C., Wapling, J., Mueller, I., Siba, P. M., and Barry, A. E. (2011) Population genetic analysis of the *Plasmodium falciparum* 6-Cys protein Pf38 in Papua New Guinea reveals domain-specific balancing selection. *Malar. J.* **10,** 126
20. Gilson, P. R., Nebl, T., Vukcevic, D., Moritz, R. L., Sargeant, T., Speed, T. P., Schofield, L., and Crabb, B. S. (2006) Identification and stoichiometry of glycosylphosphatidylinositol-anchored membrane proteins of the human malaria parasite *Plasmodium falciparum*. *Mol. Cell. Proteomics* **5,** 1286–1299
21. Taechalertpaisarn, T., Crosnier, C., Bartholdson, S. J., Hodder, A. N., Thompson, J., Bustamante, L. Y., Wilson, D. W., Sanders, P. R., Wright, G. J., Rayner, J. C., Cowman, A. F., Gilson, P. R., and Crabb, B. S. (2012) Biochemical and functional analysis of two *Plasmodium falciparum* blood-stage 6-Cys proteins. P12 and P41. *PLoS One* **7,** e41937
22. Kumar, N., and Wizel, B. (1992) Further characterization of interactions between gamete surface antigens of *Plasmodium falciparum*. *Mol. Biochem. Parasitol.* **53,** 113–120
23. Crawford, J., Grujic, O., Bruic, E., Czjzek, M., Grigg, M. E., and Boulanger, M. J. (2009) Structural characterization of the bradyzoite surface antigen (BSR4) from *Toxoplasma gondii*, a unique addition to the surface antigen glycoprotein 1-related superfamily. *J. Biol. Chem.* **284,** 9192–9198
24. Crawford, J., Lamb, E., Wasmuth, J., Grujic, O., Grigg, M. E., and Boulanger, M. J. (2010) Structural and functional characterization of SporoSAG. A SAG2-related surface antigen from *Toxoplasma gondii*. *J. Biol. Chem.* **285,** 12063–12070
25. He, X. L., Grigg, M. E., Boothroyd, J. C., and Garcia, K. C. (2002) Structure of the immunodominant surface antigen from the *Toxoplasma gondii* SRS superfamily. *Nat. Struct. Biol.* **9,** 606–611
26. Boulanger, M. J., Tonkin, M. L., and Crawford, J. (2010) Apicomplexan parasite adhesins. Novel strategies for targeting host cell carbohydrates. *Curr. Opin. Struct. Biol.* **20,** 551–559
27. Wasmuth, J. D., Pszenny, V., Haile, S., Jansen, E. M., Gast, A. T., Sher, A., Boyle, J. P., Boulanger, M. J., Parkinson, J., and Grigg, M. E. (2012) Integrated bioinformatics and targeted deletion analyses of the SRS gene superfamily identify SRS29C as a negative regulator of *Toxoplasma* virulence. *MBio* **3,** e00321–12
28. Aurrecoechea, C., Brestelli, J., Brunk, B. P., Dommer, J., Fischer, S., Gajria, B., Gao, X., Gingle, A., Grant, G., Harb, O. S., Heiges, M., Innamorato, F., Iodice, J., Kissinger, J. C., Kraemer, E., Li, W., Miller, J. A., Nayak, V., Pennington, C., Pinney, D. F., Roos, D. S., Ross, C., Stoeckert, C. J., Jr., Treatman, C., and Wang, H. (2009) PlasmoDB. A functional genomic database for malaria parasites. *Nucleic Acids Res.* **37,** D539–D543
29. Massingham, T., and Goldman, N. (2005) Detecting amino acid sites under positive selection and purifying selection. *Genetics* **169,** 1753–1762
30. Sievers, F., Wilm, A., Dineen, D., Gibson, T. J., Karplus, K., Li, W., Lopez, R., McWilliam, H., Remmert, M., Söding, J., Thompson, J. D., and Higgins, D. G. (2011) Fast, scalable generation of high-quality protein multiple sequence alignments using Clustal omega. *Mol. Syst. Biol.* **7,** 539
31. Waterhouse, A. M., Procter, J. B., Martin, D. M., Clamp, M., and Barton, G. J. (2009) Jalview Version 2. A multiple sequence alignment editor and analysis workbench. *Bioinformatics* **25,** 1189–1191
32. Tamura, K., Peterson, D., Peterson, N., Stecher, G., Nei, M., and Kumar, S. (2011) MEGA5. Molecular evolutionary genetics analysis using maximum likelihood, evolutionary distance, and maximum parsimony methods. *Mol. Biol. Evol.* **28,** 2731–2739
33. Alexander, D. L., Arastu-Kapur, S., Dubremetz, J. F., and Boothroyd, J. C. (2006) *Plasmodium falciparum* AMA1 binds a rhoptry neck protein homologous to TgRON4, a component of the moving junction in *Toxoplasma gondii*. *Eukaryot. Cell* **5,** 1169–1173
34. Leslie, A. G. W. (1992) *Joint CCP4 + ESF-EAMCB Newsletter on Protein Crystallography* No. 26
35. Evans, P. (2006) Scaling and assessment of data quality. *Acta Crystallogr. D Biol. Crystallogr.* **62,** 72–82
36. Winn, M. D., Ballard, C. C., Cowtan, K. D., Dodson, E. J., Emsley, P., Evans, P. R., Keegan, R. M., Krissinel, E. B., Leslie, A. G., McCoy, A., McNicholas, S. J., Murshudov, G. N., Pannu, N. S., Potterton, E. A., Powell, H. R., Read, R. J., Vagin, A., and Wilson, K. S. (2011) Overview of the CCP4 suite and current developments. *Acta Crystallogr. D Biol. Crystallogr.* **67,** 235–242
37. McCoy, A. J., Grosse-Kunstleve, R. W., Adams, P. D., Winn, M. D., Storoni, L. C., and Read, R. J. (2007) Phaser crystallographic software. *J. Appl. Crystallogr.* **40,** 658–674
38. Schwarzenbacher, R., Godzik, A., Grzechnik, S. K., and Jaroszewski, L. (2004) The importance of alignment accuracy for molecular replacement. *Acta Crystallogr. D Biol. Crystallogr.* **60,** 1229–1236
39. Emsley, P., and Cowtan, K. (2004) Coot. Model-building tools for molecular graphics. *Acta Crystallogr. D Biol. Crystallogr.* **60,** 2126–2132
40. Murshudov, G. N., Vagin, A. A., and Dodson, E. J. (1997) Refinement of macromolecular structures by the maximum-likelihood method. *Acta Crystallogr. D Biol. Crystallogr.* **53,** 240–255
41. Petrotchenko, E. V., Serpa, J. J., Hardie, D. B., Berjanskii, M., Suriyamongkol, B. P., Wishart, D. S., and Borchers, C. H. (2012) Use of proteinase K

nonspecific digestion for selective and comprehensive identification of interpeptide cross-links. application to prion proteins. *Mol. Cell. Proteomics* **11,** M111.013524
42. Petrotchenko, E. V., and Borchers, C. H. (2010) ICC-CLASS. Isotopically coded cleavable cross-linking analysis software suite. *BMC Bioinformatics* **11,** 64
43. Edgar, R. C. (2004) MUSCLE. Multiple sequence alignment with high accuracy and high throughput. *Nucleic Acids Res.* **32,** 1792–1797
44. Eswar, N., Webb, B., Marti-Renom, M. A., Madhusudhan, M. S., Eramian, D., Shen, M. Y., Pieper, U., and Sali, A. (2006) Comparative protein structure modeling using Modeller. *Curr. Protoc. Bioinformatics* Chapter 5, Unit 5.6
45. Pettersen, E. F., Goddard, T. D., Huang, C. C., Couch, G. S., Greenblatt, D. M., Meng, E. C., and Ferrin, T. E. (2004) UCSF Chimera. A visualization system for exploratory research and analysis. *J. Comput. Chem.* **25,** 1605–1612
46. Polley, S. D., and Conway, D. J. (2001) Strong diversifying selection on domains of the *Plasmodium falciparum* apical membrane antigen 1 gene. *Genetics* **158,** 1505–1512
47. Wickramarachchi, T., Cabrera, A. L., Sinha, D., Dhawan, S., Chandran, T., Devi, Y. S., Kono, M., Spielmann, T., Gilberger, T. W., Chauhan, V. S., and Mohmmed, A. (2009) A novel *Plasmodium falciparum* erythrocyte binding protein associated with the merozoite surface, PfDBLMSP. *Int. J. Parasitol.* **39,** 763–773
48. Beeson, J. G., Andrews, K. T., Boyle, M., Duffy, M. F., Choong, E. K., Byrne, T. J., Chesson, J. M., Lawson, A. M., and Chai, W. (2007) Structural basis for binding of *Plasmodium falciparum* erythrocyte membrane protein 1 to chondroitin sulfate and placental tissue and the influence of protein polymorphisms on binding specificity. *J. Biol. Chem.* **282,** 22426–22436
49. Tanabe, K., Escalante, A., Sakihama, N., Honda, M., Arisue, N., Horii, T., Culleton, R., Hayakawa, T., Hashimoto, T., Longacre, S., Pathirana, S., Handunnetti, S., and Kishino, H. (2007) Recent independent evolution of msp1 polymorphism in *Plasmodium vivax* and related simian malaria parasites. *Mol. Biochem. Parasitol.* **156,** 74–79
50. Williamson, K. C., and Kaslow, D. C. (1993) Strain polymorphism of *Plasmodium falciparum* transmission-blocking target antigen Pfs230. *Mol. Biochem. Parasitol.* **62,** 125–127
51. Anthony, T. G., Polley, S. D., Vogler, A. P., and Conway, D. J. (2007) Evidence of non-neutral polymorphism in *Plasmodium falciparum* gamete surface protein genes Pfs47 and Pfs48/45. *Mol. Biochem. Parasitol.* **156,** 117–123
52. Escalante, A. A., Grebert, H. M., Chaiyaroj, S. C., Riggione, F., Biswas, S., Nahlen, B. L., and Lal, A. A. (2002) Polymorphism in the gene encoding the Pfs48/45 antigen of *Plasmodium falciparum*. XI. Asembo Bay Cohort Project. *Mol. Biochem. Parasitol.* **119,** 17–22
53. van Dijk, M. R., van Schaijk, B. C., Khan, S. M., van Dooren, M. W., Ramesar, J., Kaczanowski, S., van Gemert, G. J., Kroeze, H., Stunnenberg, H. G., Eling, W. M., Sauerwein, R. W., Waters, A. P., and Janse, C. J. (2010) Three members of the 6-Cys protein family of *Plasmodium* play a role in gamete fertility. *PLoS Pathog.* **6,** e1000853
54. Escalante, A. A., Lal, A. A., and Ayala, F. J. (1998) Genetic polymorphism and natural selection in the malaria parasite *Plasmodium falciparum*. *Genetics* **149,** 189–202
55. Tetteh, K. K., Stewart, L. B., Ochola, L. I., Amambua-Ngwa, A., Thomas, A. W., Marsh, K., Weedall, G. D., and Conway, D. J. (2009) Prospective identification of malaria parasite genes under balancing selection. *PLoS One* **4,** e5568
56. Li, J., Ito, D., Chen, J. H., Lu, F., Cheng, Y., Wang, B., Ha, K. S., Cao, J., Torii, M., Sattabongkot, J., Tsuboi, T., and Han, E. T. (2012) Pv12, a 6-Cys antigen of *Plasmodium vivax*, is localized to the merozoite rhoptry. *Parasitol. Int.* **61,** 443–449
57. Moreno-Pérez, D. A., Areiza-Rojas, R., Flórez-Buitrago, X., Silva, Y., Patarroyo, M. E., and Patarroyo, M. A. (2013) The GPI-anchored 6-Cys protein Pv12 is present in detergent-resistant microdomains of *Plasmodium vivax* blood stage schizonts. *Protist* **164,** 37–48
58. Williamson, K. C., Keister, D. B., Muratova, O., and Kaslow, D. C. (1995) Recombinant Pfs230, a *Plasmodium falciparum* gametocyte protein, induces antisera that reduce the infectivity of *Plasmodium falciparum* to mosquitoes. *Mol. Biochem. Parasitol.* **75,** 33–42
59. Outchkourov, N. S., Roeffen, W., Kaan, A., Jansen, J., Luty, A., Schuiffel, D., van Gemert, G. J., van de Vegte-Bolmer, M., Sauerwein, R. W., and Stunnenberg, H. G. (2008) Correctly folded Pfs48/45 protein of *Plasmodium falciparum* elicits malaria transmission-blocking immunity in mice. *Proc. Natl. Acad. Sci. U.S.A.* **105,** 4301–4305
60. Davidson, E. A., and Gowda, D. C. (2001) Glycobiology of *Plasmodium falciparum*. *Biochimie* **83,** 601–604
61. Krissinel, E., and Henrick, K. (2007) Inference of macromolecular assemblies from crystalline state. *J. Mol. Biol.* **372,** 774–797
62. Carter, R., Coulson, A., Bhatti, S., Taylor, B. J., and Elliott, J. F. (1995) Predicted disulfide-bonded structures for three uniquely related proteins of *Plasmodium falciparum*, Pfs230, Pfs48/45, and Pf12. *Mol. Biochem. Parasitol.* **71,** 203–210
63. Holm, L., and Park, J. (2000) DaliLite workbench for protein structure comparison. *Bioinformatics* **16,** 566–567
64. Cesbron-Delauw, M. F., Tomavo, S., Beauchamps, P., Fourmaux, M. P., Camus, D., Capron, A., and Dubremetz, J. F. (1994) Similarities between the primary structures of two distinct major surface proteins of *Toxoplasma gondii*. *J. Biol. Chem.* **269,** 16217–16222
65. Lekutis, C., Ferguson, D. J., and Boothroyd, J. C. (2000) *Toxoplasma gondii*. Identification of a developmentally regulated family of genes related to SAG2. *Exp. Parasitol.* **96,** 89–96
66. Lekutis, C., Ferguson, D. J., Grigg, M. E., Camps, M., and Boothroyd, J. C. (2001) Surface antigens of *Toxoplasma gondii*. Variations on a theme. *Int. J. Parasitol.* **31,** 1285–1292
67. Jung, C., Lee, C. Y., and Grigg, M. E. (2004) The SRS superfamily of *Toxoplasma* surface proteins. *Int. J. Parasitol.* **34,** 285–296
68. Boothroyd, J. C., Hehl, A., Knoll, L. J., and Manger, I. D. (1998) The surface of *Toxoplasma*. More and less. *Int. J. Parasitol.* **28,** 3–9